Available online at www.sciencedirect.com
SCIENCE DIRECT
International Journal of Machine Tools & Manufacture 45 (2005) 1412–1420
INTERNATIONAL JOURNAL OF MACHINE TOOLS & MANUFACTURE DESIGN, RESEARCH AND APPLICATION
www.elsevier.com/locate/ijmactool

The coolant penetration in grinding with segmented wheels—part 1: mechanism and comparison with conventional wheels

T. Nguyen, L.C. Zhang*

School of Aerospace, Mechanical and Mechatronic Engineering, The University of Sydney, NSW 2006, Australia

Received 10 November 2004; accepted 28 January 2005
Available online 7 March 2005

Abstract

This paper aims to study the mechanism of coolant penetration into a wheel-work contact zone when a segmented or conventional wheel is used in surface grinding. Based on the principles of fluid motion and considerations of spin-off and splash, analytical models for both conventional and segmented wheels were developed for predicting the power of pumping coolant into the contact zone. It was revealed that the pumping power of a segmented wheel increases with the increment of wheel speed, but that of a conventional wheel decreases. It was shown that coolant minimisation in surface grinding is possible when using a segmented wheel, although its efficiency depends on the wheel speed and methods of coolant supply. The model predictions were in good agreement with experimental observations.

Keywords: Coolant minimisation; Pumping power; Segmented grinding wheel; Conventional grinding wheel; Analytical models

1. Introduction

The chemical additives in machining coolants have raised critical concerns on environmental pollution and waste disposal cost [1]. The problem becomes considerable in grinding where a large amount of coolant is often required for high surface integrity components [2,3]. Therefore, developing alternative cooling methods with less harmful coolant has been important to industry. Some investigations have also been conducted to try to replace coolant by cryogens [4,5] or by using abrasive materials of higher thermal conductivity and wear resistance [6]. However, the solutions are still far from satisfaction. The difficulty in using cryogens is its low ability to penetrate into the grinding zone due to its high evaporation rate, which limits its applicability [4]. On the other hand, spin-off and splashing of coolant in grinding, usually above 95–98% of the coolant applied, make it difficult to reduce the quantity of coolant [7].

To grind difficult-to-machine materials in creep-feed mode, Suto et al. [8] introduced a segmented grinding wheel with perforated holes to allow coolant to radially flow into the wheel-work contact zone. It was reported that this type of wheel could bring about a reduction of specific energy by 36%. However, possible coolant saving was not investigated and the mechanism of coolant penetration was unclear. The present authors made a further development by introducing a pressurised fluid chamber to enhance the flow of coolant through the perforated holes [9,10]. With such wheel system, the surface quality of ground workpieces could be improved even when the quantity of coolant applied was only 30% of that in a conventional system. Adhesion of ground chips on the wheel surface disappeared and surface tensile residual stresses caused by thermal deformation were eliminated. However, a comprehensive study of the fluid flow mechanism has not been available.

This paper aims to study the mechanisms of coolant penetration into the grinding zone associated with both the segmented and conventional grinding wheels.

2. Experimental apparatus

Fig. 1 shows the segmented grinding wheel containing 144 equally spaced CBN segments of B100P120V. An annular groove with bore holes was machined on the wheel hub to enable radial coolant flow through the space between

* Corresponding author. Tel.: +61 2 9351 2835; fax: +61 2 9351 7060.
E-mail address: zhang@aeromech.usyd.edu.au (L.C. Zhang).

0890-6955/$ - see front matter © 2005 Elsevier Ltd. All rights reserved.
doi:10.1016/j.ijmachtools.2005.01.035

Nomenclature

A	area (m^2)
b	wheel width (m)
Co	concentration number in Eq. (10)
C_c	coefficient in Eq. (22) (m^2)
C_s	coefficient in Eq. (29) (m^2)
C_ψ	dimensionless separation coefficient in Eq. (36)
d	diameter (m)
d_w	depth of cut (m)
g	gravitational constant (m/s^2)
h	equivalent liquid layer thickness in Eq. (8) (m)
H	pumping head (m)
K	constant in Eq. (34) (m)
l_{cv}	control volume arc length (Figs. 4 and 5)
l_w	wheel-work contact length (m)
M	moment (Nm)
N	total number of segments in a segmented wheel
n_{cv}	number of perforated holes within the control volume (Fig. 7)
$\vec{n}$	normal unit vector
P	pumping power (W)
Q	volume flow rate (m^3/s)
Q_t	total volume flow rate supplied to a system (m^3/s)
r	integrated radius in Eq. (12) (m)
R	radius (m)
Re	Reynolds number in Eq. (39)
S	cross-sectional area of the splashing stream in Eq. (32) (m^2)
Sc	screen number in Eq. (9)
t	thickness of coolant layer entering into the grinding zone (m)
T	pumping torque (Nm)
v	velocity (m/s)
V_w	volume of the liquid within the grinding zone (m^3)
z	boundary limit of the control volume presented in Figs. 6 and 7 (m)
α	constant in Eq. (35) (ms/rad)
β	constant in Eq. (35) (m)
γ	control volume angle (rad)
δ	spin-off liquid thickness in Eq. (34) (m)
λ	mean separated distance between the wheel grits
μ	dynamic viscosity (Ns/m^2)
ρ	coolant density (kg/m^3)
ϕ	alignment angle of the fluid chamber in Fig. 3 (rad)
ψ	separation angle (rad)
ω	rotational grinding wheel speed (rad/s)
Ω	relative velocity of the wheel to the workpiece (rad/s)

Subscripts

c	spin-off or centrifugal
cv	control volume
e	outlet
f	liquid film
g	wheel grit
h	bore hole of the segmented wheel
i	inlet
j	jet
jω	combined jet-wheel
k	individual
sp	splashing
w	wheel-work contact zone

the segments. Two different methods were used to charge the coolant into the grinding zone: (a) the free-flow method used by Suto et al. [8], where coolant was introduced by a nozzle to the wheel groove but its transportation to the grinding zone through the bore holes relied on the centrifugal force generated by wheel rotation (Fig. 2); and (b) the forced-flow method, where coolant was pressurised to flow through the bore holes within a coolant chamber installed on the wheel hub [9,10] (Fig. 3). Depending on the wheel speed, the angular position of the chamber, ϕ, can be adjusted to ensure that the coolant flow was mainly within the grinding zone. The velocities of the coolant jets through the bore holes were determined by the method of high-speed strobe photography [10].

In the case of a conventional grinding wheel of the same abrasive type and grade, coolant was provided from a nozzle placed 50 mm apart from the grinding zone with an impinging angle of 30° tangential to the workpiece surface.

The experimental parameters used in this study are given in Table 1.

3. Modelling

The effectiveness of heat removal from a grinding zone depends largely on the amount of coolant which can be

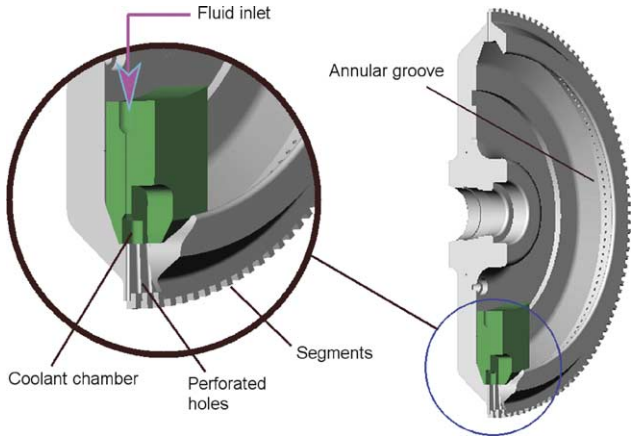

Fig. 1. Section view of the segmented wheel/fluid chamber assembly.

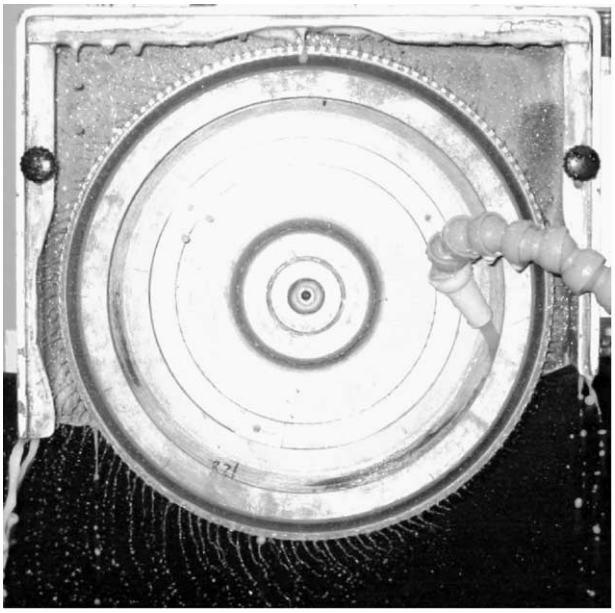

Fig. 2. Flow field of coolant in the free-flow coolant supply system.

brought into the zone, and hence relies on the pumping power of a coolant supply system. If the volumetric flow rate and the pumping head of a coolant supply system are Q and H, respectively, its pumping power P is [11,12]

$$P = \rho g Q H \tag{1}$$

where ρ is the coolant density and g is the gravitational constant.

The pumping actions of the coolant supply systems associated with the conventional and segmented wheels are shown in Figs. 4 and 5, respectively. With a sufficient volume flow rate, the surface tension and viscous force will hold a volume of coolant in the vicinity of the grinding zone inlet. Because of the relative motion between the wheel and the workpiece, pumping takes place within this volume and its power can be determined as

$$P = T\Omega \tag{2}$$

Fig. 3. Flow field of coolant in the forced-flow coolant supply system.

Table 1
Experimental parameters

Grinding machine	Minini Junior 90 CNC-M286
Grinding wheel	(a) Segmented wheel: Designation: B100P120V Radius, $R=150$ mm, 144 segments Perforated hole diameter, $d_n=2$ mm (b) Conventional wheel: Designation: B100P120V Radius, $R=150$ mm
Fluid chamber	Material: teflon (PTFE) Cross sectional area, $A_1=88.3$ mm^2 Number of perforated holes within the fluid chamber, $n=4$
Coolant	Noritake SA-02 Concentration: 1:60 Surface tension (N/m): $\approx 73.1\times10^{-3}$ (water based) Dynamic viscosity (Ns/m^2): 12.1×10^{-4} Density (kg/m^3): 980 Maximum flow rate (L/min): 18.8

where T is the pump driving torque and Ω is the rotational wheel speed relative to the movement of the workpiece v_w, i.e.

$$\Omega = \omega \pm \frac{v_w}{R} \tag{3}$$

where R is the wheel radius and the plus or minus sign corresponds to up or down grinding, respectively.

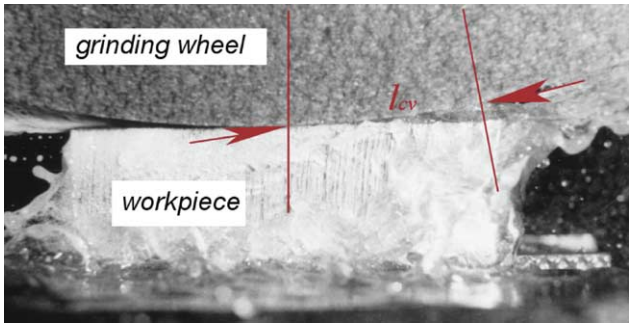

Fig. 4. Entrainment of coolant into the grinding zone using the conventional coolant supply system.

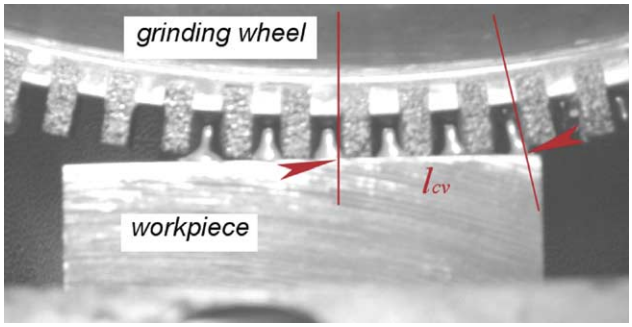

Fig. 5. Entrainment of coolant into the grinding zone using the segmented wheel.

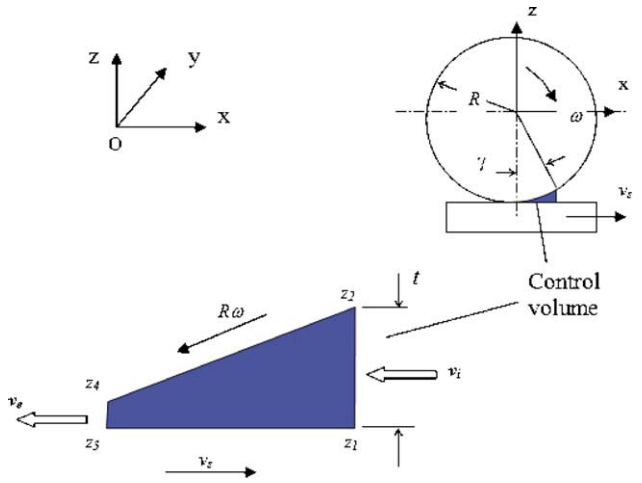

Fig. 6. Analytical control volume using the conventional coolant supply system.

The pumping performance of the conventional and segmented wheel systems will be discussed in the next few sections.

Since our purpose is to understand the mechanism difference of the two wheel systems, for simplicity but without loosing generality, we assume that the side flow of coolant perpendicular to the xz plane is negligible ($\vec{v}_y = 0$), so that the following analysis takes place within the xz coordinate plane as defined in Figs. 6 and 7.

3.1. Conventional wheel system

According to the coolant flow revealed by the experiment shown in Fig. 4, the control volume for analysis in this case can be selected as illustrated by the shaded trapezium in Fig. 6. The boundary of the control volume is defined as

$$z_1 = z_3 = -R \tag{4}$$

$$z_2 = -R\cos\gamma \tag{5}$$

$$z_4 = -(R - h) \tag{6}$$

where γ is the control volume angle determined by the measured arc length l_{cv} (Figs. 5 and 6), i.e.

$$\gamma = \frac{l_{cv}}{R}, \tag{7}$$

and h is an equivalent thickness of the coolant layer in the grinding zone. With the assumption that the wheel grits are spheres of radius R_g and separated by a mean distance λ, h can be determined by equating the volume of the liquid layer V_w (Fig. 8), i.e.

$$V_w = bl_w h$$

$$= bl_w\left\{(R_g - d_w) - \frac{\pi}{\lambda^2}\left[\frac{2}{3}R_g^3 - d_w^2\left(R_g - \frac{d_w}{3}\right)\right]\right\} \tag{8}$$

$$h = (R_g - d_w) - \frac{\pi}{\lambda^2}\left[\frac{2}{3}R_g^3 - d_w^2\left(R_g - \frac{d_w}{3}\right)\right]$$

where l_w is the wheel-work contact length, b is the wheel width, d_w the depth of cut of a grit, and R_g and λ can be obtained using the screen number Sc of the abrasive grits and their concentration Co specified by the wheel designation according to the ANSI standard B74-20 [13], i.e.

$$\mathrm{Sc}(2R_g) = 0.7(25.4\times 10^{-3}) \tag{9}$$

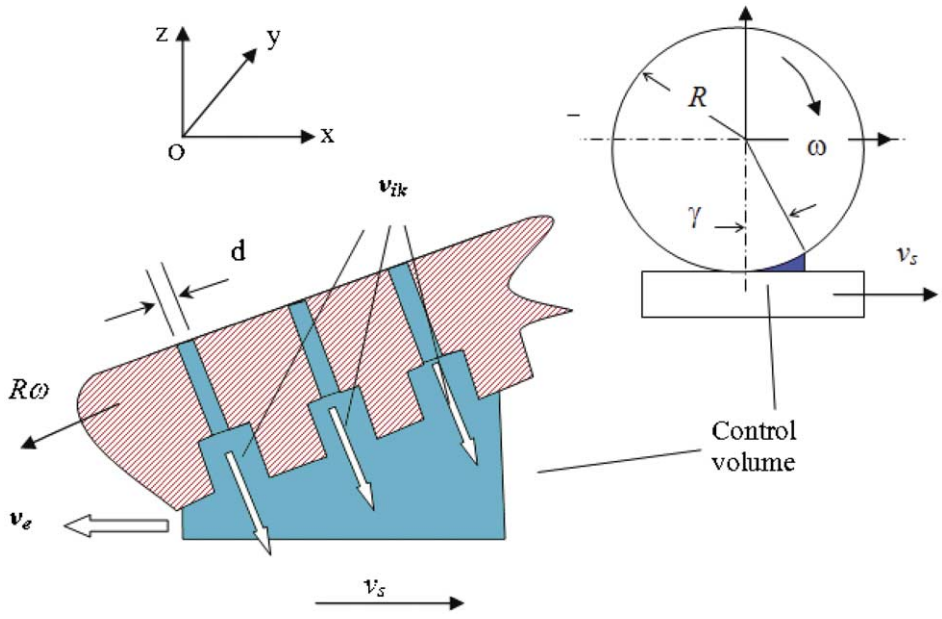

Fig. 7. Analytical control volume using the segmented wheel.

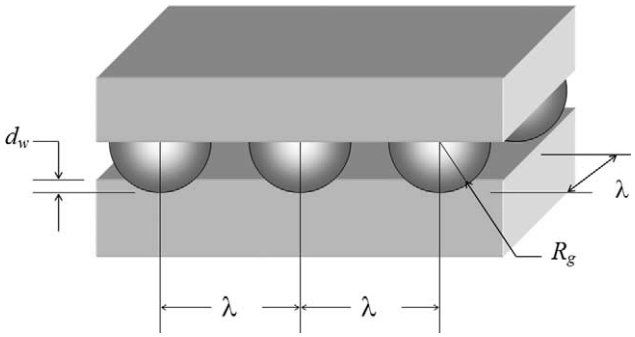

Fig. 8. Sketch of thickness h determination.

and

$$\lambda = \left[\frac{1}{0.25\times 10^{-2}\mathrm{Co}}\left(\frac{4}{3}\pi R_g^3\right)\right]^{1/3} \tag{10}$$

By using the angular momentum equation for a steady flow to the defined control volume, the pump driving torque, T, as indicated in Eq. (2), can be determined as [11,12]

$$\vec{T} = -\sum \vec{M}_y \tag{11}$$

where

$$\sum \vec{M}_y = \oint_{A_{cv}} \rho(\vec{r}\times\vec{v})_y(\vec{v}\cdot\vec{n})\,\mathrm{d}A \tag{12}$$

in which $\vec{r}$ and $\vec{v}$ are the radius and velocity vectors, respectively, and $\vec{n}$ is the unit vector normal to the inlet/outlet area A_{cv}.

At the inlet of the control volume,

$$\vec{v}\cdot\vec{n} = -v_i \tag{13}$$

and

$$|\vec{r}\times\vec{v}|_y\,\mathrm{d}A = z(v_i\cos\gamma)b\,\mathrm{d}z \tag{14}$$

At the outlet,

$$\vec{v}\cdot\vec{n} = v_e \tag{15}$$

and

$$|\vec{r}\times\vec{v}|_y dA = z v_e b dz \tag{16}$$

where v_i and v_e are the mean velocities at the inlet and outlet through the A_{cv} of the control volume, respectively (Fig. 6). The magnitude of $\sum \vec{M}_y$ therefore can be determined by substituting these into Eq. (12), i.e.

$$\begin{aligned}\sum M_y &= \int_{z_1}^{z_2}\rho(zv_i b\cos\gamma)(-v_i)\mathrm{d}z + \int_{z_3}^{z_4}\rho(zv_e b)(v_e)\mathrm{d}z \\ &= -\frac{1}{2}\rho b v_i^2(\cos\gamma)z^2\Big|_{z_1}^{z_2} + \frac{1}{2}\rho b v_e^2 z^2\Big|_{z_3}^{z_4}\end{aligned} \tag{17}$$

Then using Eqs. (4)–(6), we get

$$\sum M_y = \frac{1}{2}\rho b\left[\frac{1}{2}v_i^2R^2\sin 2\gamma\sin\gamma + v_e^2 h(-2R+h)\right] \tag{18}$$

As we have assumed that $\vec{v}_y = 0$, which is satisfied in most surface grinding cases ($R\gamma \ll b$), the continuity equation gives

$$v_e = v_i\frac{R(1-\cos\gamma)}{h} \tag{19}$$

Hence, the pumping power P of the conventional wheel can be determined by rearranging Eqs. (2), (3), (11), (18) and (19), which gives rise to

$$P = \frac{1}{2}\rho b R^2 v_i^2\Omega\left[\frac{1}{2}\sin 2\gamma\sin\gamma + (1-\cos\gamma)^2\left(\frac{2R}{h}-1\right)\right] \tag{20}$$

Since $V_s/R \ll \omega$ and from Eq. (3), $\Omega \approx \omega$, Eq. (20) reduces to

$$P = \left(\frac{1}{2}\rho R\omega\right)C_c v_i^2 \tag{21}$$

where

$$C_c = Rb\left[\frac{1}{2}\sin 2\gamma\sin\gamma + (1-\cos\gamma)^2\left(\frac{2R}{h}-1\right)\right] \tag{22}$$

can be considered as a coefficient representing the influence of the conventional wheel configuration on its pumping power of coolant.

3.2. Segmented wheel system

The control volume in this case is defined in Fig. 7. Since at the inlet of the control volume,

$$\vec{r}\times\vec{v} = 0 \tag{23}$$

the integration of Eq. (12) gives rise to

$$\sum M_y = \int_{z_3}^{z_4}\rho(zv_e b\,\mathrm{d}z)v_e = \frac{1}{2}\rho b v_e^2(-2Rh+h^2) \tag{24}$$

On the other hand, the continuity equation yields

$$v_e = \left(\frac{1}{bh}\right)\left(\frac{\pi d_h^2}{4}\right)\sum_{k=1}^{n_{cv}} v_{ik} \tag{25}$$

where v_{ik} is the velocity of individual flow discharged through a perforated hole of diameter d_h, and n_{cv} is the number of perforated holes within the control volume determined by

$$n_{cv} = \frac{N\gamma}{2\pi} \tag{26}$$

in which N is the total number of segments fitted in the grinding wheel.

Hence, Eqs. (2), (3), (11), (24) and (25) bring about

$$P = \frac{1}{2}\rho b\left(\frac{\pi d_h^2}{4}\frac{1}{b}\right)^2\Omega(2R/h-1)\left(\sum_{k=1}^{n_{cv}} v_{ik}\right)^2 \tag{27}$$

Similar to Eq. (21), Eq. (27) can also be expressed as

$$P = \left(\frac{1}{2}\rho R\omega\right) C_s \left(\sum_{k=1}^{N\gamma/2\pi} v_{ik}\right)^2 \tag{28}$$

where

$$C_s = \frac{1}{b}\left(\frac{\pi d_h^2}{4}\right)^2 \left(\frac{2R}{h} - 1\right) \tag{29}$$

can be viewed as a coefficient representing the influence of the segmented wheel configuration on its pumping power of coolant.

4. Effect of coolant splash and spin-off

In any real surface grinding with either the conventional or segmented wheel system, coolant splash and spin-off are unavoidable. These will certainly influence the quantity and velocity of coolant to enter the control volume, and consequently, affect the pumping power. This section will discuss the splash and spin-off effects.

4.1. Conventional wheel system

Fig. 9 shows the impingement of a coolant jet with diameter d_j from a nozzle. The coolant splash results in a momentum transfer and causes a flow, Q_{sp}, bifurcating from the main flow stream, Q_j. However, the viscous force and surface tension of coolant hold a liquid layer with thickness f on the wheel surface [14,15] and preserve a film flow, Q_f. The law of mass conservation then gives:

$$Q_j = Q_{sp} + Q_f \tag{30}$$

On the other hand, according to the Bernoulli's equation for a steady and incompressible flow

$$v_j = v_{sp} = v_f = v_i \tag{31}$$

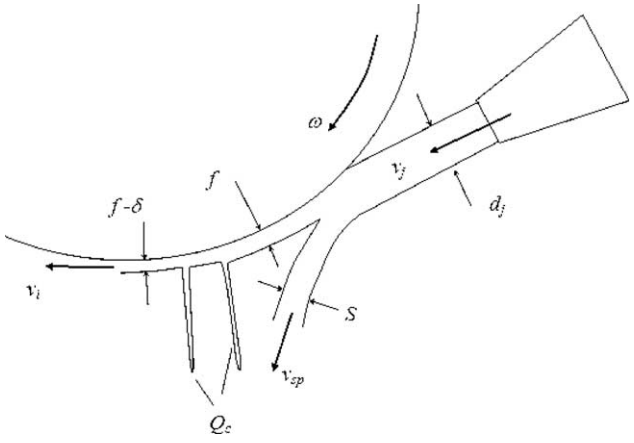

Fig. 9. Sketch of coolant impingement of the wheel surface.

where v_j, v_{sp} and v_f are the velocities of the liquid jet, splash flow and the liquid film as showed in Fig. 9, respectively, and v_i is the inlet velocity in Eq. (21).

Using the continuity law, Eqs. (30) and (31) lead to

$$\frac{\pi d_j^2}{4} = S + bf \tag{32}$$

where S is the cross-sectional area of the splashing stream.

However, due to the spin-off, the layer thickness f will be reduced by a thickness δ. Thus, the spin-off flow rate Q_c is [16,17]

$$Q_c = \delta^2 v_{j\omega} = \delta^2(v_j + 2\pi R\omega) \tag{33}$$

where

$$\delta = KC_\psi(Re^{-1/2} + 0.25) \tag{34}$$

in which K is the correction coefficient. Within the wheel speed ranging from 517 to 1982 rpm, K can be experimentally determined as [17]

$$K = \alpha\omega + \beta = 4.14 \times 10^{-11}\left(\frac{60\omega}{2\pi}\right) - 1.04 \times 10^{-8} \tag{35}$$

In Eq. (34), C_ψ is the separation coefficient defined as

$$C_\psi = \frac{1 + \cos\psi}{2} \tag{36}$$

in which

$$\psi = \tan^{-1}\left(\frac{\sin\varsigma}{1 - \cos\varsigma}\right) \tag{37}$$

and

$$\varsigma = \cos^{-1}\left(1 - \frac{d_j}{2R}\right) \tag{38}$$

and Re is the Reynolds number defined as

$$Re = \frac{\rho v_{j\omega}}{\mu} = \frac{\rho(v_j + 2\pi R\omega)}{\mu} \tag{39}$$

Thus, the flow rate Q_i that enters the pumping control volume is

$$Q_i = Q_j - Q_{sp} - Q_c \tag{40}$$

By applying the Bernoulli's equation and rearranging Eqs. (31), (32) and (40), we get

$$Q_i = btv_j = v_j\left(\frac{\pi d_j^2}{4} - S\right) - \delta^2 v_{j\omega} \tag{41}$$

where

$$t = |z_1 - z_2| = R(1 - \cos\gamma) \tag{42}$$

is the thickness of coolant layer entering the control volume (Fig. 6).

Using Eqs. (21) and (41), we obtain (see derivation details in the Appendix at the end of the paper)

$$\frac{\partial P}{\partial \omega} < 0 \tag{43}$$

This means that an increase of the wheel speed will reduce the pumping power.

4.2. Segmented wheel system

By applying the mechanical energy equation for a steady flow of coolant through the control volume shown in Fig. 10, we obtain

$$\frac{p_1}{\rho} + \frac{v_1^2}{2} + gz_1 - w = \frac{p_2}{\rho} + \frac{v_2^2}{2} + gz_2 \tag{44}$$

where p_1 and p_2, and v_1 and v_2 are the mean pressures and mean velocities at planes 1 and 2, respectively; and w represents the work done by the centrifugal force exerting on the mass of coolant under consideration [12], i.e.

$$w = \frac{\partial P_c}{\partial \dot{m}} = R\omega^2(z_1 - z_2) \tag{45}$$

where P_c is the centrifugal force power and $\dot{m}$ is the mass flow rate. Therefore, Eqs. (44) and (45) result in

$$v_{ik} = v_2 = \left[v_1^2 + 2\Delta z\left(g + \frac{f_c}{\rho}\right) + \frac{\Delta p}{\rho} \right]^{1/2} \tag{46}$$

where $\Delta z = z_1 - z_2$ is the perforated hole length, $\Delta p = p_1 - p_2$ is the pressure drop through the hole and $f_c = \rho R\omega^2$ is the centrifugal force acting on a unit coolant volume.

The differentiation of Eq. (46) with respect to ω gives

$$\frac{\partial v_{ik}}{\partial \omega} = 2\Delta z R\left[v_1^2 + 2\Delta z\left(g + \frac{f_c}{\rho}\right) + \frac{\Delta p}{\rho} \right]^{-1/2} > 0 \tag{47}$$

Then, Eq. (28) gives rise to

$$\frac{\partial P}{\partial \omega} = \frac{1}{2}\rho R C_s \left[\left(\sum_{k=1}^{n} v_{ik} \right)^2 + \omega \sum_{k=1}^{n} \frac{\partial v_{ik}}{\partial \omega} \right] \tag{48}$$

because γ in Eq. (28) is not a function of ω. This equation shows that

$$\frac{\partial P}{\partial \omega} > 0 \tag{49}$$

which clearly indicates that with the segmented wheel, an increase of the wheel speed will increase the pumping power. This is just opposite to the performance of the conventional wheel as concluded by Eq. (43).

5. Performance comparison

Eqs. (21) and (28) can be used to examine the variation of pumping power with different coolant supply configurations.

5.1. Segmented wheel without the chamber

In this case, the coolant supply configuration is shown in Fig. 2. The coolant flow through the perforated holes is due to the centrifugal force generated by wheel rotation. For convenience, we call it a free-flow.

Fig. 11 compares the performance of the segmented wheel with that of a conventional wheel. It shows that within the test range of wheel speed from 500 to 1500 rpm, there exists a critical wheel speed of about 1000 rpm, below which the performance of the segmented wheel is worse than the conventional wheel. In addition, as shown in Fig. 2, an over flow of coolant through the entire periphery of the wheel occurs, causing significant spin-off and wastage. Although the coolant penetration can be enhanced by using

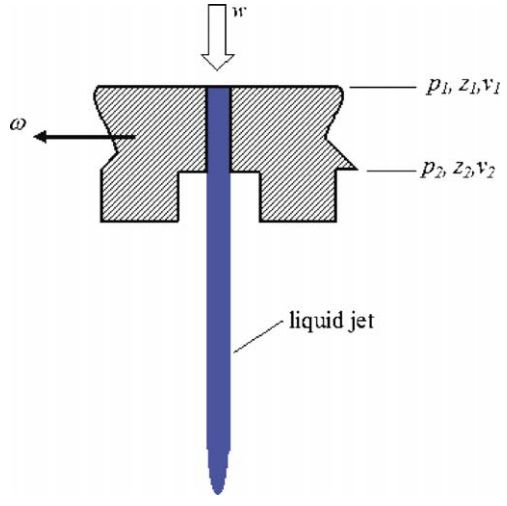

Fig. 10. Sketch of coolant jet flowing through a perforated hole.

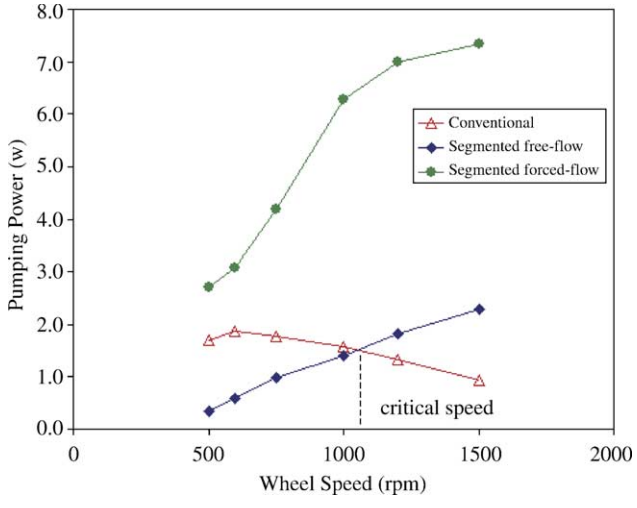

Fig. 11. Variation of the pumping power with wheel speed, $Q = 12$ L/min.

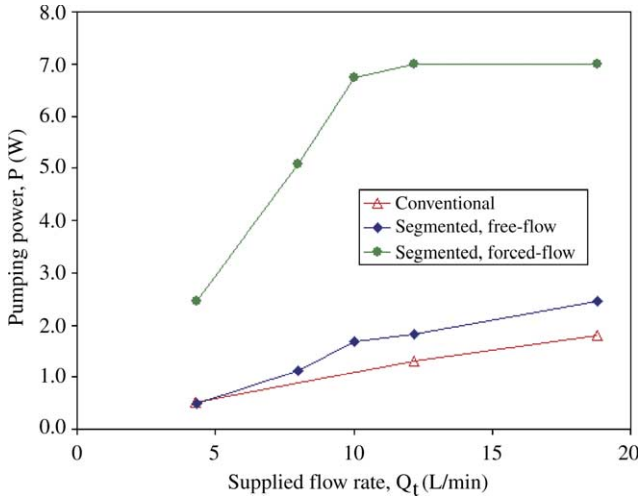

Fig. 12. Variation of the pumping power with the supplied flow rate, ω= 1200 rpm.

a high wheel speeds much above the critical speed, significant coolant mist will be generated [10].

The variation of the pumping power with the total amount of coolant supplied is shown in Fig. 12. The segmented wheel can only increase the pumping power very little. It is clear that this coolant supply method (free-flow) is not favourable.

5.2. Segmented wheel with the chamber

The configuration of the coolant supply system in this case is shown in Figs. 1 and 3. By using the coolant chamber to control coolant flow into the grinding zone, thus increasing its pressure [10], the pumping power (P) is increased significantly, as shown in Fig. 11. This indicates that the segmented wheel/chamber system is sensible in grinding practice, particularly when a high speed operation [13,18] is required.

In comparison with the performance of the conventional wheel as shown in Fig. 12, the segmented wheel with chamber can save a large amount of coolant at a high speed operation. For instance, when ω = 1200 rpm, this system can reach the same pumping power as that of a conventional wheel with only 30% of coolant flow rate.

6. Conclusions

Two analytical models have been developed to provide a physical understanding of the mechanisms of coolant penetration into the grinding zone using segmented and conventional wheels. It is concluded that coolant minimisation is possible using the segmented wheel and the efficiency depends on the wheel speed and method of coolant supply. The model provides the foundation for further quantitative studies to be carried out in the second part of the series study.

Acknowledgements

This work was supported by the Australia Research Council (ARC). The authors appreciate very much Mr Y.L. Pai and Mr J. Huang at Kinik Grinding Wheel Corp. for making the wheel segments.

Appendix

$\partial P/\partial\omega$ with a conventional wheel system

As derived in Section 3.1, the pumping power with a conventional wheel is

$$P = \left(\frac{1}{2}\rho R\omega\right) C_c v_i^2 \tag{A1}$$

where

$$C_c = Rb\left[\frac{1}{2}\sin 2\gamma \sin\gamma + (1-\cos\gamma)^2\left(\frac{2R}{h}-1\right)\right] \tag{A2}$$

Since $v_i = v_j$ (Eq. (31)), Eqs. (21) and (22) bring about

$$P = \frac{1}{2}\rho b R^2 v_i^2 \omega\left[\frac{1}{2}\sin 2\gamma \sin\gamma + (1-\cos\gamma)^2\left(\frac{2R}{h}-1\right)\right] \tag{A3}$$

The control volume governed by angle γ is affected by the splash and spin-off of coolant. According to the analysis in Section 4.1, it can be determined as

$$Q_i = btv_j = v_j\left(\frac{\pi d_j^2}{4} - S\right) - \delta^2 v_{j\omega} \tag{A4}$$

where

$$t = |z_1 - z_2| = R(1-\cos\gamma) \tag{A5}$$

Hence,

$$bR(1-\cos\gamma)v_j = v_j\left(\frac{\pi d_j^2}{4} - S\right) - \delta^2(v_j + 2\pi R\omega) \tag{A6}$$

On the other hand, from Eqs. (34), (35) and (39),

$$\delta = KC_\psi(Re^{-1/2} + 0.25) \tag{A7}$$

$$K = \alpha\omega + \beta = 4.14\times10^{-11}\left(\frac{60\omega}{2\pi}\right) - 1.04\times10^{-8} \tag{A8}$$

$$Re = \frac{\rho v_{j\omega}}{\mu} = \frac{\rho(v_j + 2\pi R\omega)}{\mu} \tag{A9}$$

Therefore,

$$\delta = C_\psi(\alpha\omega + \beta)\left\{\left[\frac{\rho(v_j + 2\pi R\omega)}{\mu}\right]^{-1/2} + 0.25\right\} \tag{A10}$$

and

$$\frac{\partial\delta}{\partial\omega} = C_{\psi}[(Re^{-1/2} + 0.25)\alpha - K\pi RRe^{-3/2}] \tag{A11}$$

For a wheel speed between 517 and 1982 rpm, the substitution of numerical values gives

$$\frac{\partial\delta}{\partial\omega} > 0 \tag{A12}$$

Hence, according to Eq. (A6),

$$\frac{\partial\gamma}{\partial\omega} = -\frac{1}{bR\sin\gamma}\left(2v_{j\omega}\delta\frac{\partial\delta}{\partial\omega} + 2\pi R\delta^2\right) < 0 \tag{A13}$$

Finally, because γ is small, Eq. (A3) leads to

$$\frac{\partial P}{\partial\omega} \approx \frac{1}{4}\rho R^2 b v_j^2 \gamma\left[3 + (1 - 4\gamma^2)^{1/2}\right]\frac{\partial\gamma}{\partial\omega} < 0 \tag{A14}$$

References

[1] I.A. Greaves, Respiratory health of automobile workers exposed to metal working fluid aerosols: respiratory symptoms, American Journal of Industrial Medicine 32 (5) (1997) 450–459.

[2] L.C. Zhang, M. Mahdi, Applied mechanics in grinding, part IV: the mechanism of grinding induced phase transformation, International Journal of Machine Tools and Manufacture 35 (10) (1995) 1397–1409.

[3] M. Mahdi, L.C. Zhang, Applied mechanics in grinding, part V: thermal residual stresses, International Journal of Machine Tools and Manufacture 37 (5) (1997) 619–633.

[4] T. Nguyen, L.C. Zhang, An assessment of the applicability of cold air-oil mist in surface grinding, Journal of Materials Processing Technology 140 (1–3) (2003) 224–230.

[5] T. Nguyen, L.C. Zhang, The effect of liquid nitrogen at surface grinding on the microstructure of a quenchable steel, in The 7th International Conference on the Progress of Machining Technology (ICPMT), 2004, Suzhou, China, p. 699–704.

[6] S. Kohli, C. Guo, S. Malkin, Energy partition to the workpiece for grinding with aluminum oxide and CBN abrasive wheels, Transactions of the ASME 117 (1995) 160–168.

[7] T. Tawakoli, Minimum coolant lubrication in grinding, Industrial Diamond Review 1 (2003) 60–65.

[8] T. Suto, T. Waida, H. Naguchi, H. Inoue, High performance creep feed grinding of difficult-to-machine materials, Bulletin of the Japan Society of Precision Engineering 24 (1) (1990) 39–44.

[9] L.C. Zhang, T. Nguyen, B. Oliver, A grinding wheel assembly and a method of grinding, Patent Application No. 20044901614, Australia.

[10] T. Nguyen, L.C. Zhang, Modelling of the mist formation in a segmented grinding wheel system, International Journal of Machine Tools and Manufacture 45 (1) (2005) 21–28.

[11] R.H. Sabersky, A.J. Acosta, E.H. Hauptmann, Fluid Flow: A First Course in Fluid Mechanics, third ed, Macmillan Publishing Company, New York, 1971.

[12] P. Gerhart, R. Gross, J. Hochstein, Fundamentals of Fluid Mechanics, second ed, Addison-Wesley Publishing Company, Reading, MA, 1992.

[13] M.C. Shaw, Principles of Abrasive Processing, Oxford University Press, UK, 1996.

[14] L. Preziosi, D. Joseph, The run-off condition for coating and rimming flows, Journal of Fluid Mechanics 187 (1988) 99–133.

[15] A.H. Lefebvre, Atomization and Spray, Combustion-an International Series, Hemisphere Publisher Corporation, Washington, DC, 1989.

[16] D.H. Wolf, F.P. Incropera, R. Viskanta, Jet impingement boiling, Advances in Heat Transfer 23 (1993) 1–132.

[17] D.D. Bell, J. Chou, S. Liang, Modeling of the environmental effect of cutting fluid, Tribology Transactions 42 (1) (1999) 168–173.

[18] L.C. Zhang, T. Suto, H. Noguchi, T. Waida, An overview of applied mechanics in grinding, Manufacturing Review 5 (4) (1992) 261–273.